CHEMICAL AND PROCESS ENGINEERING
2009, 30, 267–278

MICHAŁ KARCZ*

PREDICTION OF THE ELECTRIC CURRENT FLUX IN A TUBULAR FUEL CELL BY MEANS OF A 1D MODEL

Energy Conversion Department, Institute of Fluid Flow Machinery
Polish Academy of Sciences, Gdańsk

Numerical analysis of a tubular solid oxide fuel cell has been presented. A proposed one-dimensional model for prediction of the vector of electric current with simultaneous three-dimensional levels of continuity, momentum, energy and species transport modelling have been employed. Local changes of the current density and temperature along the fuel cell tube have been predicted. It is shown that for higher values of the average current density throughout the cell, change of relevant local values of current density has a linear slope in the axis direction and temperature field becomes more uniform.

Przedstawiono wyniki obliczeń dla pojedynczej rurki ogniwa paliwowego zasilanego wodorem. Analizę oparto na opracowanym przez autora jednowymiarowym modelu numerycznym wytwarzania prądu elektrycznego w wysokotemperaturowym, rurkowym ogniwie paliwowym. Model ten, uzupełniony trójwymiarowymi równaniami transportu masy, pędu i energii, zaimplementowano do standardowego kodu numerycznego oraz zweryfikowano według danych eksperymentalnych dla podstawowych charakterystyk ogniwa. Pokazano, że dla większych średnich wartości gęstości prądu zmiany lokalnej gęstości prądu wzdłuż rurki stają się liniowe, a rozkład temperatury – równomierny.

1. INTRODUCTION

Recently there has been an unprecedented progress in numerical modelling methods employed in a fuel cell design [1]. A detailed review of the solid oxide fuel cell (SOFC) modelling problems is given in [2, 3]. Numerical models are dedicated mainly for prediction of the temperature field to avoid dangerous thermal stresses that can cause cracking of solid-state electrolyte [4]. Electrical characteristics are also dependent on temperature field through the relevant transport processes and thermodynamic parameters.

One-dimensional modelling is the most popular way of prediction of the current density vector. In such a method, the fuel cell tube is divided into several segments by planes perpendicular to its axis. Then, an electric circuit is solved individually for

*E-mail: michal.karcz@imp.gda.pl

every single segment [1, 5–11]. Similar technique coupled via the computational fluid dynamics (CFD) technique with a 3D geometrical model is also employed in the present paper.

The model is to some extent based on previous investigations of the author concerning numerical modelling of tubular solid oxide fuel cells [12–14], however in the present paper estimation of the local current density by means of the 1D technique has been elaborated.

A commercial CFD solver Fluent [15] has been employed for a numerical implementation by means of user defined subroutines. Only one tubular fuel cell configuration of Siemens–Westinghouse design has been analyzed [6, 7]. At the first step, the numerical results have been compared with the literature experimental data. In the next step, local changes of current density and temperature in the axis direction have been discussed.

2. DESCRITPION OF THE MODEL

2.1. CURRENT FLUX MODELLING

The following electrochemical reactions occur in a fuel cell fuelled with humidified hydrogen, i.e. reduction and oxidation, at the cathode and anode, respectively:

$$\frac{1}{2}\mathrm{O_2} + 2\mathrm{e^-} \longrightarrow \mathrm{O^{2-}} \tag{1}$$

$$\mathrm{H_2} + \mathrm{O^{2-}} \longrightarrow \mathrm{H_2O} + 2\mathrm{e^-} \tag{2}$$

The ions/electrons transfer due to reactions (1) and (2) results in a flow of electric current. Charge transferred per time per the surface area is represented through current density. The current flux $\vec{i}$ can be expressed with the formula originating from the classical Ohm law [2, 16]:

$$\vec{i} = -\sigma \mathrm{grad}\phi \tag{3}$$

where the conductivity σ is a material property depending on temperature, and symbol ϕ represents the potential of the electric field.

Simplified, one-dimensional model of current density vector gives a possibility of computing local changes of current density in axial direction of a tubular fuel cell. The model used in the present study employs assumption of a constant terminal cell voltage as a potential difference between cathode and anode interconnectors [16]. Such an assumption is valid as far as there is a sufficiently low electrical resistance of interconnectors and nickel felts [6]. It should be underlined that the current flux is not considered on the same numerical grid as for the main governing equations. The tube is

additionally discretized into several segments n, as in Fig. 1, where all parameters necessary for prediction the local current density can be assumed as circumferentially uniform. In the present analysis, the segments number $n = 20$, the same as in [11], has been employed as sufficient for detailed prediction of local behaviour of the current density.

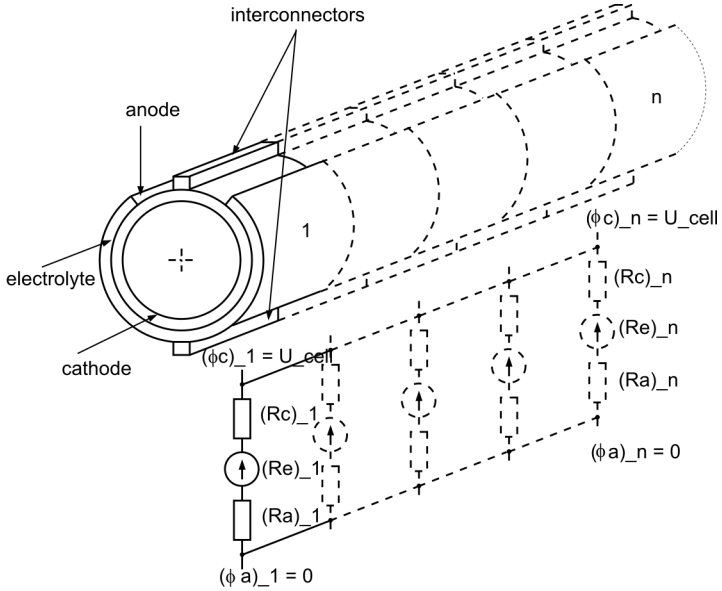

Fig. 1. Scheme of discretization of a tubular fuel cell for the 1D electrical field prediction

The classical Nernst formulation can help in estimation of local theoretical voltage U° generated in a hydrogen fed fuel cell due to elementary reactions (1) and (2) [2, 3, 7, 8, 17]:

$$U^\circ = \frac{-\Delta G^\circ}{2F} + \frac{RT}{2F}\ln\left(\frac{X_{\mathrm{H_2}} X_{\mathrm{O_2}}^{0.5}}{X_{\mathrm{H_2O}}}\right) + \frac{RT}{4F}\ln\left(p_0\right) \tag{4}$$

The operating voltage U is always lower than the theoretical one due to some polarizations [17]. Three main loss mechanisms are usually included during modelling, namely activation, concentration and ohmic losses. The operating cell voltage is then:

$$U = U^\circ - \sum_i \eta(i) = U^\circ - \left[\eta_{\mathrm{act}}(i) + \eta_{\mathrm{0ohm}}(i) + \eta_{\mathrm{conc}}(i)\right] \tag{5}$$

where i represents the axial component of the vector $\vec{\imath}$ at a specified segment n.

In the nominal range of operation of a fuel cell, only activation and ohmic losses are important, while concentration polarizations are usually neglected [7, 17]. However, at high reaction rates, the concentration polarization governs the cell operation

due to dilution of substrates and products and species transport blocking. Detailed description of the method of estimation particular polarizations in function of the current density, one can find in [1, 7, 17] or in papers of the author [12, 14].

In the present analysis, local changes of the axial component i of electric flux $\vec{i}$ are obtained implicitly using Eqs. (4) and (5).

2.2. FLUID FLOW MODEL

A mathematical model is based on the elementary balance equations solved within the frame of the finite volume method (FVM). Set of equations can be given in the following compact with CFD form [18]:

$$\frac{\partial}{\partial T}\begin{Bmatrix} \varepsilon\rho \\ e\rho\vec{v} \\ \varepsilon\rho e + (1-\varepsilon)\rho_s e_s \\ \varepsilon\rho Y_k \end{Bmatrix} + \mathrm{div}\begin{Bmatrix} \varepsilon\rho\vec{v} \\ e\rho\vec{v}\otimes\vec{v} \\ \varepsilon\rho e + (1-\varepsilon)\rho_s e_s \\ \varepsilon\rho Y_k \end{Bmatrix} + \mathrm{div}\begin{Bmatrix} 0 \\ \varepsilon p\vec{I} \\ \varepsilon p\vec{v} \\ 0 \end{Bmatrix} = \mathrm{div}\begin{Bmatrix} 0 \\ \varepsilon\vec{\tau} \\ \varepsilon\vec{\tau}\vec{v} + \vec{q} \\ \varepsilon\vec{J}_k \end{Bmatrix} + \begin{Bmatrix} \varepsilon\rho S_m \\ \varepsilon\rho\vec{S}_v \\ \varepsilon\rho S_e \\ \varepsilon\rho S_k \end{Bmatrix} \tag{6}$$

where t is time, ρ – density, $\vec{v}$ – velocity vector, Y_k – mass fraction of species k, e – total energy, p – pressure, $\vec{\vec{I}}$ – Gibbs' idemfactor, $\vec{\vec{\tau}}$ – total diffusive momentum flux, $\vec{q}$ – total diffusive heat flux, $\vec{J}_k$ – diffusive flux of species k, S_m – mass source, $\vec{S}_v$ – momentum source, S_e – energy source, S_k – creation/destruction source of a species k. Subscripts f and s refer to fluid and solid, respectively. The porosity factor ε is defined as a parameter indicating the amounts of fluid volume V_f in the finite volume V [15]:

$$\varepsilon = \frac{V_f}{V} \tag{7}$$

Creation and destruction terms S_m, S_e and S_k in the continuity, energy and species transport equations are specified as the local current density functions in the form similar as presented in [12]. The term $\vec{S}_v$ includes Darcy's force acting as an additional source in the momentum equation.

Set of Eqs. (6) is solved in a similar manner as for standard fluid-flow processes with chemical reactions. Some special treatment of diffusive transport of species inside porous structure of fuel cell electrodes is however needed. Transport of species inside the fuel cell is usually dependent on three main diffusion mechanisms, i.e.: molecular diffusion in gas channels, Knudsen diffusion and Darcy's pressure-driven flow

in the porous electrodes [3]. Three independent microstructure parameters determine diffusive transport whenever porous domain is considered, i.e. porosity ε defined via Eq. (7), tortuosity τ and mean radii of pores $\overline{r}$ [19]. In the simplest form, the diffusive flux $\vec{J}_k$ can be calculated based on the gradient hypothesis employing Fick's law [2]. Multicomponent nature of diffusion inside porous electrodes is included via the effective diffusion coefficient D_k^{eff} that accounts influence of molecular D_k^m and Knudsen diffusion D_k^K according to formula given by Yakabe et al. [20]:

$$\frac{1}{D_k^{\text{eff}}} = \frac{\tau}{\varepsilon}\left(\frac{1-\alpha_k x_k}{D_k^m} + \frac{1}{D_k^K}\right) \tag{8}$$

where the coefficient α_k is defined as:

$$\alpha_k = 1 - \left(\frac{M_k}{\overline{M}}\right)^{1/2} \tag{9}$$

The Knudsen diffusivity has the standard form as in [19]:

$$D_k^K = \frac{2}{3}\overline{r}\sqrt{\frac{8RT}{\pi M_k}} \tag{10}$$

Molecular diffusion coefficient D_k^m is calculated based on binary diffusivities D_{kl} through the simplified formula [7, 10, 20, 21]:

$$D_k^m = \frac{1-X_k}{\sum\limits_{k\neq l}\frac{X_l}{D_{kl}}} \tag{11}$$

The binary diffusion coefficients can be either derived based on the Chapman –Enskog theory or can be directly taken from Yuan and Sunden [21]. Todd and Young [22] proved that in the high temperature of operation (T > 1000 K) the Fuller et al. method is more accurate for prediction binary diffusivities D_{kl} than any other model. Details of the method one can find in [23]. Similar method as in the present analysis is employed also in [7, 8].

3. COMPUTATIONS

3.1. MODEL IMPLEMENTATION

The described model has been implemented into commercial Fluent solver using the user subroutines technique (UDF) [15]. The numerical grid for CFD calculations has been created based on the Siemens–Westinghouse design [6, 7, 9]. Basic dimensions are shown in Fig. 2. Due to symmetry of the computational domain, only a half of the tube has been considered. Discretization of the fuel cell tube has been per-

formed by means of finite volumes. The density of the grid has been assumed based on sensitivity studies for a pure flow problem without any electrochemical reactions.

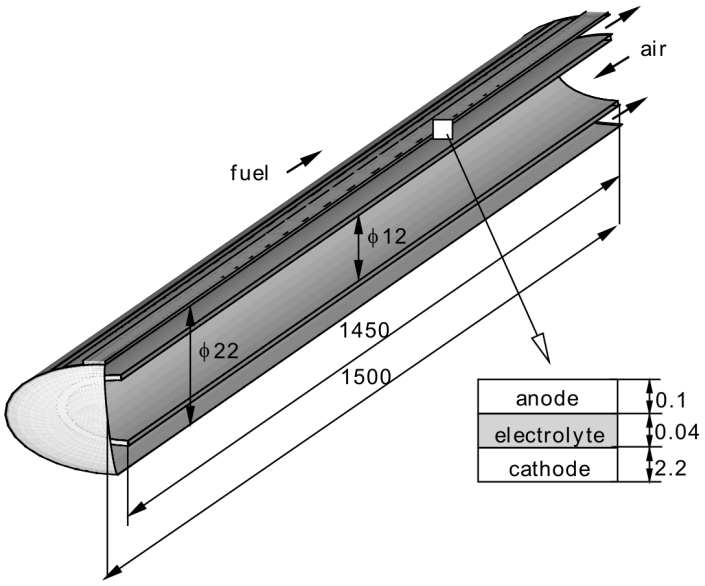

Fig. 2. Basic geometry ofa tubular fuel cell (not in scale)

Ideal gas mixture and incompressible and laminar flow have been assumed during the computations. No radiative heat transfer has been considered in this study. It should be remembered, however, that radiation leads to overall lowering of the tube temperature [9].

Properties of cathode (perovskite $LaSrMnO_3$), electrolyte (yttria-stabilized zirconia – YSZ), anode (cermet Ni-YSZ), and interconnector (doped $LaCrO_3$) materials have been adopted from various literature sources. Resistivity ρ of elements of fuel cells was taken from Zhang et al. [24]. Thermal conductivities λ of electrodes, electrolyte and interconnector have been assumed the same as by Lin and Beale [16], and for air injection tube a formula from Campanari and Iora [7] has been employed.

It has been assumed that the structure of electrodes is homogeneous and isotropic. In the present analysis, the porosity value $\varepsilon = 0.5$, tortuosity factor $\tau = 3$ and pore radius $\bar{r} = 1$ μm for both cathode and anode electrodes have been employed as in [7]. The permeability of electrodes, i.e. the parameter for Darcy's force estimation, has been determined by the Kozeny–Carman relationship [9, 10].

3.2. DISCUSSION OF THE RESULTS

Some validation of the model can be done through the current–voltage characteristics which are often available. In the present study, the data by Zhang et al. [24] and

Suwanwarangkul et al. [9] have been employed. Boundary conditions for considered case are given in Table 1.

Table 1. Composition of fuel and oxidizer, temperature at the cell inlet and global utilization factors necessary for mass flow rate estimation [9, 24]

Fuel	hydrogen	$Y_{H_2} = 0.89$	$T^f = 1123$ K	Fuel utilization factor – 0.850
	steam	$Y_{H_2O} = 0.11$		
Oxidizer	oxygen	$Y_{O_2} = 0.23$	$T^{ox} = 873$K	Oxidizer utilization factor – 0.167
	nitrogen	$Y_{N_2} = 0.77$		

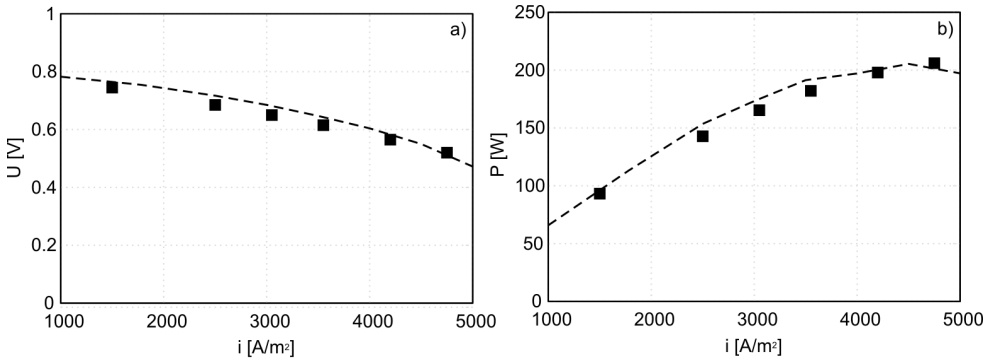

Fig. 3. Main characteristics of a single fuel cell tube: a) average current density–voltage, b) average current density – power; squares – experimental data from [24], dashed line – numerical model

Comparisons between numerical and experimental data are presented in Fig. 3 for current–voltage and current–power characteristics. Generally a good agreement between numerical and experimental data is observed in the presented range of average current densities i_{avg} for both characteristics. The computed values of voltage and power are, however, somewhat higher than the experimental ones in the range of 2500–4000 A/m^2. Similar trend has also been noticed by Zhang et al. [24].

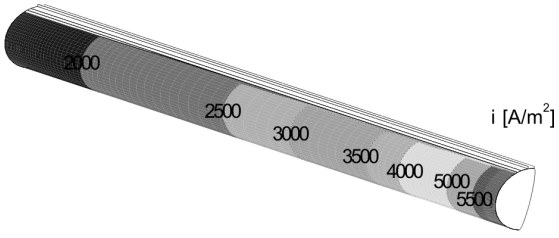

Fig. 4. Distribution of a local current density at the surface of the electrolyte of a tubular fuel cell for i_{avg} = 3000 A/m^2

In Figure 4, current density distribution at the electrolyte surface of the fuel cell tube is shown for i_{avg} = 3000 A/m^2. For the whole range of the considered average

current density a drop of its local value in the axial direction is observed. Results are quite similar to those presented by Li and Suzuki [5] where also a steady current density drop in the downstream direction is observed. On the other hand there are some discrepancies when comparison is done with data presented for example by Song et al. [11] and Suwaranwangkul et al. [9]. These differences can be explained however with different type of utilized fuel. In the present analysis a humidified hydrogen is used, while in [11] reformed gas has been considered. Different temperature distribution throughout the cell is expected then.

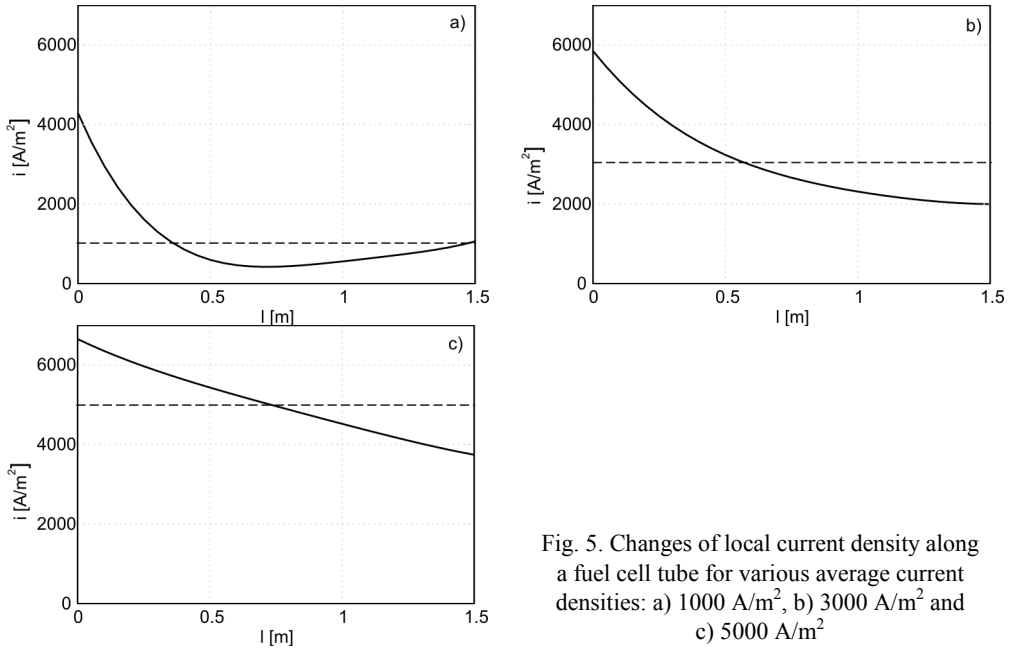

Fig. 5. Changes of local current density along a fuel cell tube for various average current densities: a) 1000 A/m^2, b) 3000 A/m^2 and c) 5000 A/m^2

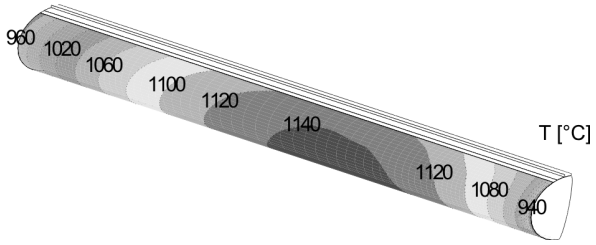

Fig. 6. Distribution of static temperature at the electrolyte surface of a fuel cell tube for i_{avg} = 3000 A/m^2

The local changes of current density for different average values in the axis direction of fuel cell tube are presented in Fig. 5. For lower average values as for example for the case of i_{avg} = 1000 A/m^2 shown in Fig. 5a the axial distribution of the current density is strongly nonlinear. However, when higher average values of current densi-

ties are considered, the relevant local changes tend to be linearly dependent on the tube length. It is especially pronounced in Fig. 5c for i_{avg} = 5000 A/m^2.

The temperature distribution is a critical element as far as it governs the level of thermomechanical stresses throughout the cell. The temperature distribution at the electrolyte surface is presented in Fig. 6 for the case i_{avg} = 3000 A/m^2. Temperature field changes in a way similar to the results presented in [6, 9, 11, 24]. As usually, the temperature maximum is located in the middle of the tube. Lower values at the fuel cell inlet and exit are due to the cooling effects of fuel and air streams, respectively.

In Figure 7, the values of the static temperature along the fuel cell for various average current densities are presented. The highest overall temperature is observed for lower values of the average current density (Fig. 7a). For higher reaction rates, increasing stream of air cools the fuel cell tube more intensively, thus its average temperature decreases. On the other hand, the exhaust temperature increases upon increasing current density. The maximum temperature shifts toward fuel cell exit for higher reaction rates (Figs. 7 b, c). For such a case the temperature distribution becomes also more uniform across the cell.

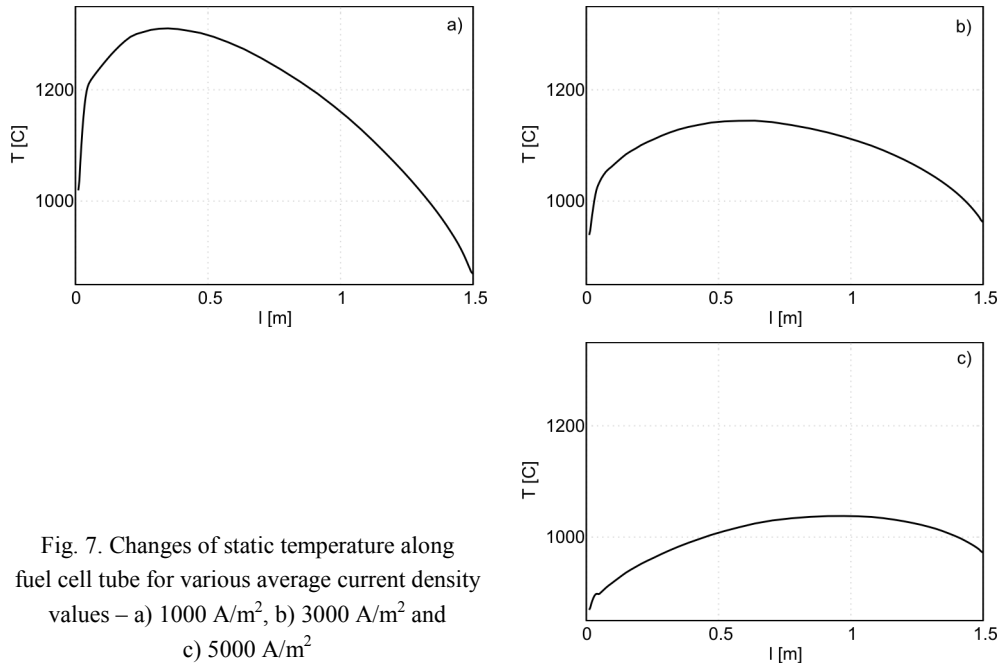

Fig. 7. Changes of static temperature along fuel cell tube for various average current density values – a) 1000 A/m^2, b) 3000 A/m^2 and c) 5000 A/m^2

4. CONCLUSIONS

One-dimensional model of the electrical current transport implemented in the present analysis gives a view inside tubular fuel cell behaviour for various loadings. An agreement with basic experimental data in the form of current density/voltage and current density/power has been noticed for a single tube. Temperature distribution at

the electrolyte surface agreed with numerical predictions presented by various authors. A possibility of prediction of the local current density has been also shown. For increasing electrochemical reaction rate, rather a linear drop of local current density has been observed in the axial direction. It is directly coupled with simultaneous flattening the values of static temperature throughout the cell.

ACKNOWLEDGEMENTS

The author expresses his gratitude to Prof. J. Badur and Dr. M. Lemański for their support on this work.

SYMBOLS

B – permeability, m^2/s
D – diffusivity coefficient, m^2/s
F – Faraday constant, C/mol
e – total energy, J/kg
$\overleftrightarrow{I}$ – Gibbs' idemfactor
$\vec{\imath}$ – electric current flux, A/m^2
$\vec{J}$ – diffusive flux of mixture component, kg/m^2s
M – molecular weight, kg/kmol
$\bar{M}$ – mean molecular weight, kg/kmol
P – power, W
p – pressure, Pa
$\vec{q}$ – total diffusive heat flux, W/m^2
$\bar{r}$ – mean pore radius, m
R – gas constant, J/(molK)
T – temperature, K
t – time, s
U – voltage, V
$\vec{v}$ – velocity vector, m/s
X – mole fraction
Y – mass fraction
ε – porosity factor
ϕ – electric field potential, V
η – polarization, V
σ – electrical conductivity, 1/(Ωm)
ρ – density, kg/m^3
τ – tortuosity factor
$\overleftrightarrow{\tau}$ – total diffusive momentum flux, Pa

SUBSCRIPTS AND SUPERSCRIPTS

° – standard, referential
a – anode
act – activation
avg – average
c – cathode
conc – concentration
e – electrolyte

eff – effective
f – fuel
k, *l* – components of mixture
ohm – ohmic
ox – oxidizer
V – momentum

REFERENCES

[1] BHARADWAJ A., ARCHER D.H., RUBIN E.S., ASME J. Fuel Cell Sci. Technol., 2005, 2, 38 .
[2] KAKAC S., PRAMUANJAROENKIJ A., ZHOU X. Y., J. Hydrogen Energy, 2007, 32, 761 .
[3] KEE R.J., ZHU H., GOODWIN D.G., Proc. Combustion Inst., 2005, 30, 2379 .
[4] KHALEEL M.A., LIN Z., SINGH P., SURDOVAL W., COLLIN D., J. Power Sources, 2004, 130, 136 .
[5] LI P.-W., SUZUKI K., J. Electrochem. Soc., 2004, 151, A548 .
[6] JIA J., ABUDULA A., WEI L., JIANG R., SHEN S., J. Power Sources, 2007, 171, 696 .
[7] CAMPANARI S., IORA P., J. Power Sources, 2004, 132, 113 .
[8] SÁNCHEZ D., CHACARTEGUI R., MUÑOZ A., SÁNCHEZ T., J. Power Sources, 2006, 160, 1074 .
[9] SUWANWARANGKUL R., CROISET E.AND PRITZKER M.D., FOWLER M.W., DOUGLAS P.L., ENTCHEV E., J. Power Sources, 2006, 154, 74 .
[10] ZHU H., KEE R.J., J. Power Sources, 2007, 169, 315 .
[11] SONG T.W., SOHN J.L., KIM J.H., KIM T.S., S.T. RO, SUZUKI K., J. Power Sources, 2005, 142, 30 .
[12] KARCZ M., Chem. Proc. Eng., 2006, 27, 201 (in Polish) .
[13] KARCZ M., Chem. Proc. Eng., 2007, 28, 307 .
[14] LEMAŃSKI M., KARCZ M., Chem. Proc. Eng., 2008, 29, 233 .
[15] User's guide, Fluent Inc., Lebanon, USA, 2005.
[16] LIN Y., BEALE S.B., App. Math. Model., 2006, 30, 1485 .
[17] NOREN D.A., HOFFMAN M.A., J. Power Sources, 2005, 152, 175 .
[18] BADUR J., *Numerical modelling of sustainable combustion in gas turbines*, IFFM Publishers, Gdańsk, 2003, (in Polish).
[19] LEHNERT W., MEUSINGER J., THOM F., J. Power Sources, 2000, 87, 57 .
[20] YAKABE H., HISHINUMA M., URATANI M., MATSUZAKI Y., YASUDA I., J. Power Sources, 2000, 86, 423 .
[21] YUAN J., SUNDEN B., ASME J. Fuel Cell Sci. Technol., 2005, 2, 38 .
[22] TODD B., YOUNG J.B., J. Power Sources, 2002, 110, 186 .
[23] REID R.C., SHERWOOD T.K., *The Properties of Gases and Liquids*, McGraw-Hill Book Company, New York, 1966.
[24] ZHANG X., LI G., LI J., FENG Z., Energy Conversion and Management, 2007, 48, 977 .

MICHAŁ KARCZ

WYZNACZANIE LOKALNYCH ZMIAN GĘSTOŚCI PRĄDU W RURKOWYM OGNIWIE PALIWOWYM NA PODSTAWIE MODELU JEDNOWYMIAROWEGO

Przedstawiono wyniki analizy stałotlenkowego ogniwa paliwowego zasilanego wodorem, którą wykonano z wykorzystaniem jednowymiarowego modelu wektora gęstości prądu. Można przyjąć, że zastosowanie takiego modelu w przypadku ogniw o budowie rurkowej jest uzasadnione, gdyż wymiar rurki w kierunku osiowym jest znacznie większy od pozostałych wymiarów. W modelu wykorzystuje się podstawowe równania bilansowe rozwiązywane metodą objętości skończonych na zdyskretyzowanej trój-

wymiarowej geometrii ogniwa. Równania transportu uzupełniono o odpowiednie człony źródłowe oraz domknięcia strumieni dyfuzyjnych. Szczegółowo opisano metodę obliczania współczynników dyfuzji w ośrodkach porowatych z uwzględnieniem parametrów geometrycznych, takich jak porowatość ε, krętość τ oraz średni wymiar porów $\bar{r}$. Wektor gęstości prądu wyznaczano na dodatkowej siatce dyskretyzującej złożonej z 20 segmentów w kierunku osiowym. W każdym segmencie uśredniano parametry niezbędne do wyznaczania napięcia teoretycznego zgodnie z równaniem Nernsta oraz polaryzacji aktywacyjnej, stężeniowej i przewodzenia generowanych w pracującym ogniwie. Ze względu na dobrą przewodność interkonektorów założono dodatkowo stałe napięcie w kierunku osiowym. Uzyskano dobrą zgodność wyników obliczeń oraz danych eksperymentalnych dla ogniwa rurkowego firmy Siemens –Westinghouse. Rozkład temperatury na powierzchni elektrolitu także odpowiada danym literaturowym. Obliczona składowa osiowa gęstości prądu się zmniejsza wraz z długością ogniwa. Stwierdzono też, że wraz ze wzrostem obciążenia ogniwa lokalne zmiany gęstości prądu w kierunku osiowym stają się liniowe. Jest to bezpośrednio związane z wyrównywaniem się temperatury dla wyższych średnich gęstości prądu.

Received 24 November, 2008